

# A portable, low-cost real-time imaging slab gel electrophoresis system for rapid separation of nucleic acids

Kan Luo <sup>a,b,\*<sup>1</sup></sup>, Yu Chen <sup>b,c,1</sup>, Min Fan <sup>d</sup>, Jianxing Li <sup>a,b</sup>, Wu Wang <sup>e</sup>

<sup>a</sup> School of electronic, Electrical engineering and Physics, Fujian University of Technology, Fuzhou 350118, China

<sup>b</sup> Fuzhou Industrial Integration Automation Technology Innovation Center, Fuzhou 350118, China

<sup>c</sup> School of Mechanical and Automotive Engineering, Fujian University of Technology, Fuzhou 350118, China

<sup>d</sup> Fujian Provincial Key Laboratory for Advanced Micro-nano Photonics Technology and Devices, Institute for Photonics Technology, Quanzhou Normal University, Quanzhou 362000, China

<sup>e</sup> College of Electrical Engineering and Automation, Fuzhou University, Fuzhou 350108, China

## ARTICLE INFO

### Keywords:

Slab gel electrophoresis (SGE)

Portable system

Real-time imaging

Fluorescence-based detection

DNA analysis

## ABSTRACT

**Background:** Slab gel electrophoresis (SGE) remains fundamental to biomedical research but faces limitations for point-of-care testing due to its large footprint, operational inefficiencies, and lack of real-time imaging capabilities.

**Methods:** We developed a portable, real-time imaging SGE system featuring a compact and modular design. The system integrates a 3D-printed SGE tank with embedded quartz glass plates that facilitate fluorescence imaging and efficient heat dissipation, ensuring stable operation under high electric fields without significant temperature rise. A uniform LED panel provides consistent, high-quality excitation, while a smartphone-based detection module with an optical filter enables real-time monitoring of fluorescent bands across a large imaging area ( $100 \times 60 \text{ mm}^2$ ).

**Results:** The SGE system offers efficient passive heat dissipation and enables sensitive fluorescence-based DNA detection, with a detection limit as low as  $0.07 \text{ ng}/\mu\text{L}$  and a linear range of  $0.08\text{--}10.00 \text{ ng}/\mu\text{L}$ . It supports a throughput of 12 samples per run. Its compact size ( $108 \times 108 \times 60 \text{ mm}^3$ ), light weight (0.7 kg), and low cost (~\$65) ensure both portability and affordability. We have successfully applied the prototype to screen genes (CERK1 and CEBP), achieving a reduced electrophoresis runtime of 12 min at 100 V while enabling real-time band tracking.

**Significance:** Our portable SGE system addresses critical limitations of traditional systems through its integrated design, large imaging area, high efficiency, and cost effectiveness. The open source platform enables both accessibility in developing regions and extensibility to diverse molecular detection applications. The established engineering approaches offer a generalizable reference for developing similar devices.

## 1. Introduction

Slab gel electrophoresis (SGE) is a ubiquitous tool for the separation and analysis of nucleic acids and proteins in genetics, molecular biology, biochemistry, and forensic science [1–5], and serves as an essential step in extraction, cloning, and PCR workflows [6,7]. Despite its widespread use and versatility, traditional SGE system are not well suited for resource-limited settings or point-of-care testing (POCT). They often require bulky equipment, including heavy power supplies and UV-based gel imaging systems, and are time-consuming in operations, which

sometimes taking several hours to complete [8]. Moreover, conventional gel documentation is typically an end-point process, separated bands are only visualized after the run by dedicated benchtop imagers [9]. These constraints become particularly problematic in POCT and resource-limited environments where compactness, operational simplicity, rapid analysis, and real-time detection are essential. Therefore, there remains a significant unmet need for cost-effective, portable and rapid SGE solutions to support on-site analyses.

Recent efforts to enhance SGE portability and efficiency have focused on device miniaturization through advanced fabrication techniques, and

\* Corresponding author at: School of electronic, Electrical engineering and Physics, Fujian University of Technology, Fuzhou 350118, China.

E-mail address: [luokan@fjut.edu.cn](mailto:luokan@fjut.edu.cn) (K. Luo).

<sup>1</sup> These authors contributed equally to this work

electric field intensification to accelerate separations. Several groups have demonstrated the potential of microfabricated systems, including stereolithographic 3D-printed microchips with 50  $\mu\text{m}$  cross-sections [10], stacked-printed microfluidic channels ( $48 \times 12 \mu\text{m}^2$ ) [11], and biochip-based platforms achieving 50 bp DNA ladder resolution within 14 min [12]. While these miniaturized systems successfully address size and cost constraints, their operation at elevated electric fields for faster separation introduces significant thermal management challenges. The Joule heating effects are exacerbated by the use of low-thermal-conductivity polymers (PDMS, PMMA, polycarbonate) [13–16], which result in temperature rise, leading to detrimental effects including: band resolution loss, separation efficiency reduction, analyte decomposition, or even gel melting [17–22]. To address thermal challenges in miniaturized systems, researchers have developed both active and passive cooling strategies. Active cooling approaches, such as thermoelectric systems [23] and Peltier-based temperature control [24], can maintain stable operation under high electric field strength (up to 63 V/cm) while improving detection sensitivity by 10-fold. Passive methods, including structural modifications to chips [25], have demonstrated 3-fold resolution improvements during rapid (30-second) separations. However, these solutions often add complexity and cost while compromising portability.

To improve the efficiency of SGE, parallel efforts have been made to integrate imaging capabilities for real-time monitoring and analysis during electrophoresis [26,27]. Imaging integration not only enhances analytical efficiency but also avoids issues such as sample contamination that may arise from removing the gel for post-processing, thereby improving overall reliability. Recent advancements have expanded fluorescent detection from spots to surfaces, and increased imaging areas from  $1 \text{ cm}^2$  to  $7 \times 7 \text{ cm}^2$ , enabling higher throughput, broader dynamic range, and improved limit of detection (LOD) [28–31]. Researchers have begun addressing these limitations by developing miniaturized SGE platforms with integrated real-time imaging. Notably, chip-based SGE devices coupled with smartphone cameras have been shown to separate DNA ladders in minutes while allowing live monitoring of band migration [32]. Likewise, fully 3D-printed gel electrophoresis devices powered by battery have demonstrated rapid protein separations comparable to benchtop systems, with results captured via a mobile phone [33]. While such approaches enhance versatility and sensitivity, they introduce elaborate mechanical and electronic control, or complex optical setups, such as multi-LED arrays [30] and precise angular alignment [31], reducing the ease-of-use and robustness in field conditions. In short, achieving broader imaging coverage or ultra-low LOD often comes at the cost of a more complicated setup. Consequently, truly portable SGE systems that combine real-time imaging with simplicity and reliability remain an unsolved challenge.

In light of these challenges, we present a new portable real-time imaging SGE system to balance analytical performance with field-ready portability. The motivation for this work is to create a compact, modular, and low-cost platform that enables SGE in decentralized settings without sacrificing speed or sensitivity. Our system features a fully 3D-printed enclosure that miniaturizes the entire electrophoresis apparatus. Uniquely, it employs quartz glass plates as part of the gel tank, which serves dual purposes: providing a clear window for fluorescence imaging and simultaneously dissipating Joule heat from the gel. A custom LED irradiation module provides uniform excitation across a large  $100 \times 60 \text{ mm}^2$  gel area, allowing standard agarose gels to be visualized. For detection, we integrate a smartphone-based camera module with an inexpensive optical filter, forming a low-cost fluorescence imaging setup capable of real-time, continuous monitoring of DNA bands. Importantly, the device uses only passive cooling, as the thermal conductivity of the quartz plates obviate any need for active cooling fans or bulky heat management. By combining these innovations, the prototype system maintains high sensitivity and throughput of 12 samples per run, while being lightweight, self-contained, and inexpensive. This work thus bridges the gap between

laboratory-grade SGE and point-of-care needs, delivering a practical solution for on-site molecular analysis.

The major contributions of our work include:

- Compact, open source design: We developed a fully 3D-printed, modular SGE system with a small footprint and low fabrication cost (~ \$65), enabling easy assembly, portability, and accessibility in resource-limited settings.
- Dual-function quartz glass plates: The integration of quartz plates allows both high-quality fluorescence imaging and efficient passive heat dissipation, ensuring stable operation at high electric field strength without active cooling.
- Uniform large-area irradiation: A custom LED panel provides consistent excitation across a  $100 \times 60 \text{ mm}^2$  gel area, supporting high detection sensitivity and throughput without complex optics.
- Smartphone-based real-time detection: A simple detection module combining a smartphone and an optical filter enables real-time monitoring of fluorescent bands over a large area, offering performance comparable to benchtop systems at a fraction of the cost.
- High-field rapid electrophoresis under passive cooling: The system supports rapid DNA separations (12 min @100 V for 12 samples) with reliable real-time imaging, demonstrated through successful screening of rice receptor protein kinase genes.

## 2. Materials and methods

The modular architecture of the portable real-time imaging SGE system, which mainly consists of five integrated components (Fig. 1): (1) a rechargeable lithium battery enabling field operation; (2) a 520 nm filter and an SGE separation tank with quartz glass; (3) a multifunctional power supply module simultaneously driving electrophoresis and LED excitation; (4) an LED panel module for uniform excitation; and (5) a smartphone and some peripheral accessories including a flexible octopus tripod and connection cables. The modular architecture allows for quick assembly, easy maintenance and reliable performance in the laboratory or in the field. [Supplementary materials S1 - S3](#) provide additional resources, including the open source project repository, a summary of the bill of materials, and design file documentation.

### 2.1. Design and fabrication of SGE tank

The SGE tank was designed using SOLIDWORKS (version 2021), featuring inert alloy flat electrodes, and an embedded quartz glass plate for efficient heat dissipation and high-quality fluorescence imaging. The tank comprises four main components (Fig. 1A): an insulating cover, a pair of flat electrodes, a quartz glass plate, and an outer shell. Both the cover and shell were fabricated via UV-curable resin 3D printing. A pair of platinum-titanium alloy electrodes ( $100 \times 20 \times 1 \text{ mm}^3$ ) is chosen to minimize biochemical reactions and ensure a uniform electric field. The electrodes are spaced 80 mm apart, while a  $60 \times 100 \times 1 \text{ mm}^3$  quartz glass plate is embedded in bottom of the shell, positioned 20 mm from the cathode. The fully assembled tank measures  $108 \times 108 \times 25 \text{ mm}^3$ .

### 2.2. FEM simulation model of SGE tank

Finite element method (FEM) simulation was used to further analyze and optimize the heat distribution in the tank. The electronic potential  $V$  is governed by the equation of Poisson [34]:

$$\nabla \cdot (\epsilon \nabla V) = -\rho_f \quad (1)$$

where  $\epsilon$  is the permittivity of the material, such as electrode, gel, or buffer.  $\rho_f$  is the free charge density. In regions where  $\rho_f = 0$ , Eq. (1) can be reduced to:

$$\nabla^2 V = 0 \quad (2)$$

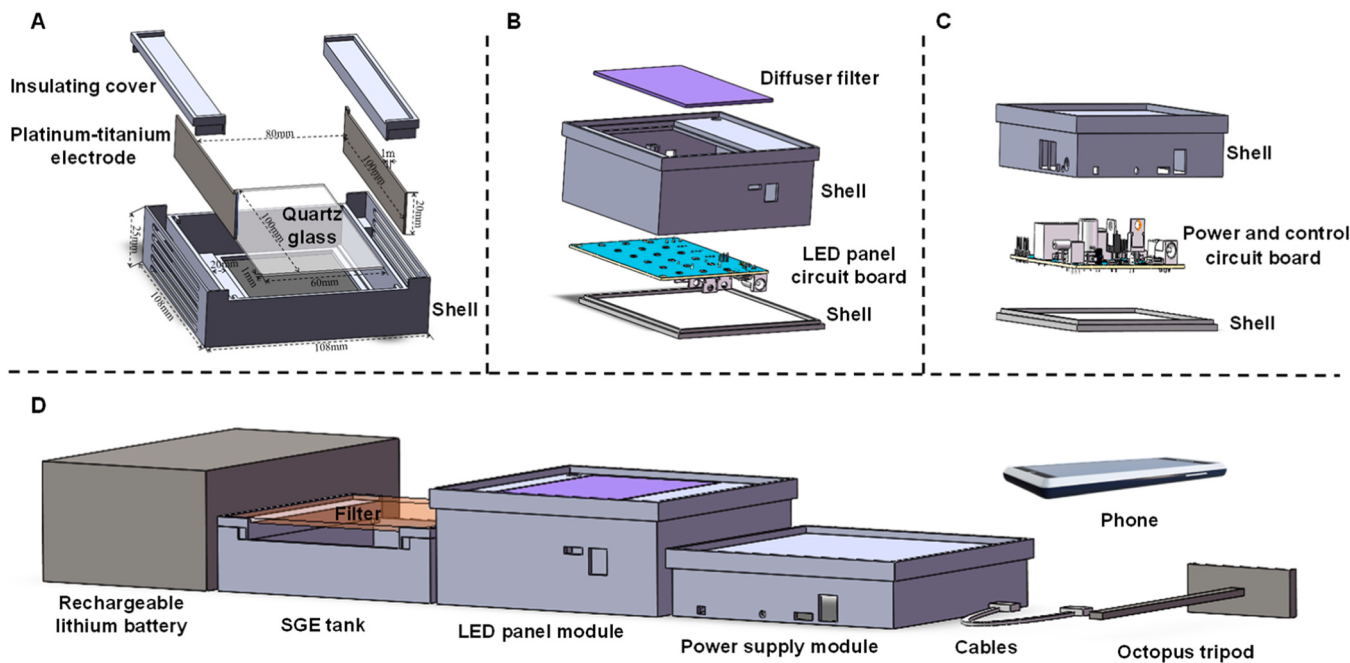


**Fig. 1.** The 3D schematic of the proposed SGE system. (A) - (C) are exploded views of the SGE tank, LED panel module and power supply module, respectively. (D) presents a separated 3D view of all system modules.

and, the electric field strength  $E$  can be derived from the gradient of the potential  $V$ :

$$E = -\nabla V \quad (3)$$

During the GE run, heat transfer in the tank is described by the equation [35]:

$$\rho c_p u \cdot \nabla T = \nabla \cdot (k \nabla T) + Q_{Joule} \quad (4)$$

where  $\rho$ ,  $c_p$ , and  $u$  are the density of different materials, heat capacity at constant pressure, and velocity of fluid, respectively,  $\nabla T$  is the temperature gradient,  $k$  is the heat conductivity, and  $Q_{Joule}$  is the Joule heat generated. In our FEM simulation of the SGE tank, the geometric model for temperature distribution is configured as a three-dimensional representation, with dimensions matching the actual model. There is no liquid flow, so  $u = 0$ . The Joule heat  $Q_{Joule}$  is dynamically calculated based on the following equation.

$$Q_{Joule} = J \cdot E \quad (5)$$

$$J = \sigma E \quad (6)$$

In Eq. (5) and Eq. (6),  $E$  is electric field strength,  $J$  is current density vector, and  $\sigma$  is electrical conductivity.

The main parameters for the FEM simulation of the SGE tank are provided in [Table 1](#). And the simulation results, along with a comparison to the heat dissipation performance of prototype system are presented in [Section 3](#). Based on finite element analysis, we confirmed that the

proposed SGE tank design, featuring a quartz glass plate and flat electrodes, offers excellent heat dissipation and can operate stably under high electric field strength conditions.

### 2.3. Large-area imaging and irradiation evenness optimization

High-quality, high-throughput electrophoresis imaging demands a wide and uniformly illuminated imaging area. Recent advances in smartphone image sensor technology have demonstrated promising results in scientific imaging applications [32]. Inspired by these developments, we used a smartphone (iPhone 13 Pro) to capture fluorescence images. The smartphone's advanced CMOS sensor, complemented by powerful image processing software, ensures superior image quality and reliable performance, facilitating accurate fluorescence image analysis.

In the irradiation design, we adopted a backlighting approach with an LED panel positioned directly under the quartz glass embedded in the SGE tank (as shown in Fig. 2). To ensure uniform irradiation, we optimized key parameters, including the distance between the LED panel and the gel ( $z$ ), the spacing between the two LEDs ( $d$ ), and the arrangement of the LED array ( $a \times b$ ). As shown in Fig. 2, the light intensity generated by the LED light source chip placed at the spatial point A ( $x_s, y_s, z_s$ ) at the target plane point B( $x, y, z$ ) can be expressed as [36]:

$$I(x, y, z) = z^{K+1} \cdot I_0 \cdot ((x - x_s)^2 + (y - y_s)^2 + (z - z_s)^2)^{-\frac{K+3}{2}} \quad (7)$$

**Table 1**  
Main FEM simulation parameters for SGE tank optimization design

	Electricity		Heat		
	Permittivity	Conductivity [S/m]	Thermal Conductivity [ $\text{W m}^{-1} \text{K}^{-1}$ ]	Thermal Diffusivity [ $\text{mm}^2 \text{s}^{-1}$ ]	Heat Capacity [ $\text{J g}^{-1} \text{K}^{-1}$ ]
Quartz glass	-	-	1.262	0.792	1.593
UV-curable resin	-	-	0.350	0.312	1.739
Electrodes	$1\text{e}^8$	$5\text{e}^6$	62.500	0.532	0.293
10X TBE buffer	78	$5.5\text{e}^{-3}$	0.590	0.143	4.200
Agarose gel , 1 %	80	$6.8\text{e}^{-4}$	0.530	0.144	4.180

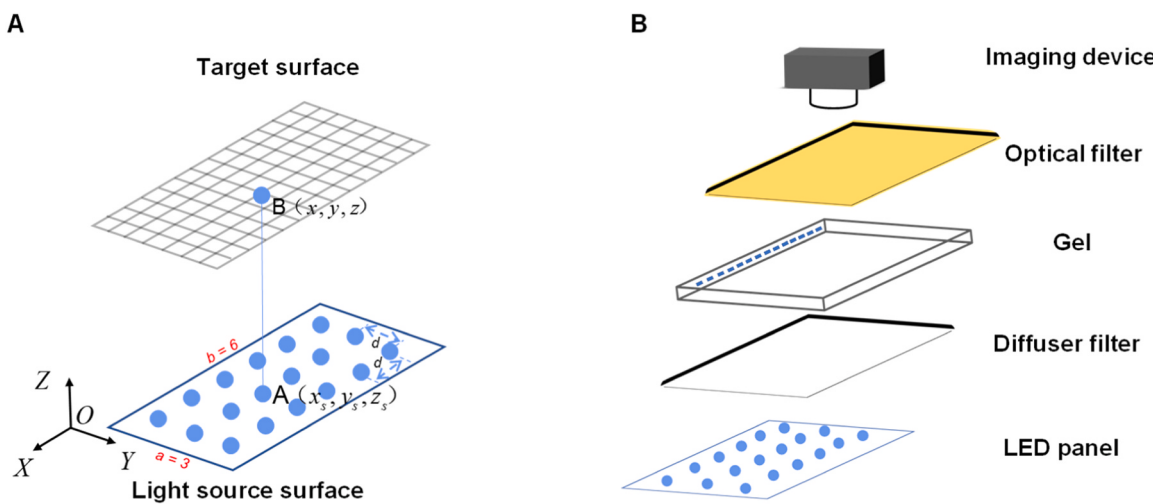


**Fig. 2.** Schematic of the LED light source. (A) LED array configuration. Each LED panel consists of multiple LED beads arranged in a  $3 \times 6$  array, with a spacing of  $d$  between adjacent LEDs. The LED panel is positioned at a distance  $z$  from the flat gel, providing vertical irradiation. (B) Schematic of the online imaging system. All optical components are assembled together to form a complete inline imaging system.

where  $I$  is the light intensity on the target plane,  $I_0$  is the light intensity on the axis, and  $K$  is the light source radiation mode, which is a constant when the half-intensity angle remains unchanged [37].

Since light emitted by the LED array is incoherent, the total intensity at any target point equals the sum of individual LED contributions [38]. We determine the optimal  $z$ -value using a two-LED configuration. The intensity distribution from this array is expressed as [36]:

$$I(x, y, z) = z^{K+1} \cdot I_0 \cdot \left( \left( \left( x - \frac{d}{2} \right)^2 + y^2 + z^2 \right)^{-\frac{K+3}{2}} + \left( \left( x + \frac{d}{2} \right)^2 + y^2 + z^2 \right)^{-\frac{K+3}{2}} \right) \quad (8)$$

where  $d$  represents the distance between the two LEDs.

If  $\frac{d^2 I}{dx^2} = 0$ , and  $x = 0, y = 0$ , that:

$$z = \sqrt{\frac{K+4}{4}} \cdot d \quad (9)$$

The optimal distance  $z$  between the LED panel and the gel is determined by the values of  $K$  and  $d$ , where  $K$  is a constant that depends on the half-intensity angle of the LED light source. In this study, we used 18 LEDs with a center wavelength of 450 nm and a half-intensity angle of  $60^\circ$  ( $K = 1$ ) [36]. These LEDs are arranged in a  $3 \times 6$  array with  $d = 17.8$  mm spacing on a flat panel. Based on Eq. (9), the optimal distance between the LED panel and the gel is calculated as  $z = 20$  mm.

The performance of the LED panel and fluorescence detection were evaluated in terms of irradiation evenness [31] and LOD [39], respectively. And LOD was calculated using the following equations:

$$LOD = k \times s/b \quad (10)$$

Where  $s$  is the standard deviation of the blank measures,  $k$  is a numerical factor chosen according to the confidence level desired, and according to IUPAC document [39]  $k$  is 3. And  $b$  is the sensitivity, a slope of the linear calibration curve of the relationship between concentration and fluorescence band intensity,

$$y = a + b \times c \quad (11)$$

where  $c$  and  $a$  are concentration and intercept, respectively.

#### 2.4. Reagents, samples, and buffers

Speed-STAR HS DNA Polymerase, 2000 bp DNA marker, and 10000X SYBR Green I were purchased from Takara (Shanghai, China). 1X TBE buffer (1X TBE = 89 mM Tris / 89 mM boric acid / 2 mM EDTA, pH = 8.4) and agarose powder were purchased from Solarbio (Beijing, China). The 1.0 % agarose gel was prepared by dissolving 0.25 g of agarose in

25 mL of 1X TBE buffer, heating to complete dissolution and cooling to  $\sim 55^\circ\text{C}$  before adding 1  $\mu\text{L}$  of 10000X SYBR Green I dye. The gel was poured into the electrophoresis disc and solidify to a height of  $\sim 4$  mm. The primers for rice receptor protein kinase genes (CERK1 and CEBP), and heat shock protein genes (HSP70) in kelp, were synthesized by Sangon Biotech (Shanghai, China). Hydroxyethyl cellulose (HEC, 1300 k) was purchased from Polysciences (Warrington, PA, USA). All samples and buffers were prepared in Milli Q water (18.2  $\text{M}\Omega\text{ cm}$ , Merck Millipore, USA).

For all experiments, gels were prepared using approximately 25 mL of the 1 % agarose gel solution, with 60 mL of 1X TBE buffer as the electrophoresis medium. A total of 3–5  $\mu\text{L}$  of pre-prepared sample solution was loaded into each lane using a precision pipette (SAIEISE, 0.5–10  $\mu\text{L}$ ). The power consumption was measured with a microampere-level power meter (Amakia EKA1080B, China). To quantify the intensity of the DNA bands, images were analyzed using Image J (<https://imagej.nih.gov/ij/>), which uses 8-bit pixel values (grayscale values) for measurement.

## 3. Results

### 3.1. The real-time imaging SGE prototype system

The real-time imaging SGE prototype system adopts a modular design for enhanced portability and functionality (Fig. 3). From bottom to top, the system consists of a power supply module, a rechargeable lithium battery, an LED panel module, a SGE tank, a 520 nm bandpass

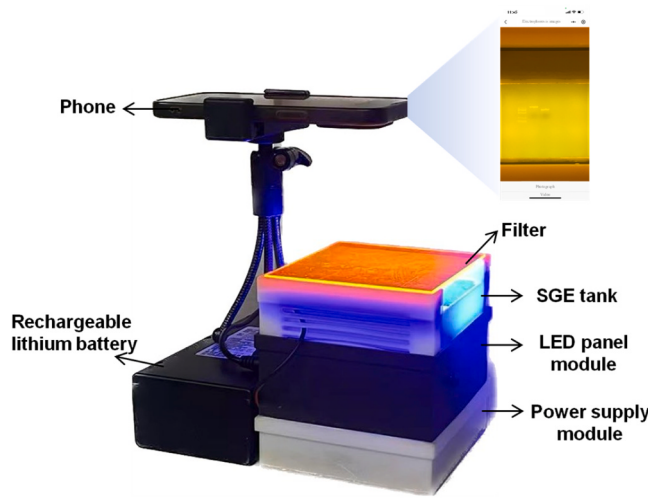


**Fig. 3.** The prototype of the proposed real-time imaging SGE system.

filter, and a mobile phone. The rechargeable lithium battery powers the system. The power supply module, controlled by a microcontroller, converts the energy of lithium battery to drive both the LED panel and the SGE tank. Particularly, it uses a BOOST converter circuit (LM5022) to supply 24–140 V to the SGE tank, generating an electric field strength of 3–17.5 V/cm. The LED panel module, equipped with eighteen 465 nm LEDs and a diffuser, ensures uniform irradiation across the SGE tank. During operation, the LED array emits excitation light through the glass plate into the SGE tank, triggering fluorescence in the dye of gel. A mobile phone with a CMOS camera, positioned 10 cm above the tank, captures real-time images or videos of the electrophoresis process. Positioned between the camera and the tank, a 520 nm bandpass filter effectively suppresses non-specific fluorescence, resulting in clear, high-contrast images. The entire system is compact and lightweight, measuring  $108 \times 108 \times 60 \text{ mm}^3$ , weighing approximately 0.7 kg, and costs approximately \$65, making it highly portable and cost-effective. The components of the prototype system, including the SGE tank shield, power supply housing, and LED panel module casing, were designed using SolidWorks and fabricated using a 3D printer (HM-300S, Hotmine 3D, Korea). Additional system specifications are provided in **Table 2**, and detailed circuit information is available in supplementary section S3.

### 3.2. Passive heat dissipation and accelerated separation

High electric field strength accelerates nucleic acid separation in SGE, but at the same time increases system temperature [17,18]. To evaluate the thermal performance and passive heat dissipation capacity of our custom-designed SGE tank, which is critical for preventing gel melting under high electric field strength, we performed numerical simulations and experimental measurements at a maximum applied

**Table 2**  
Specifications of the proposed real-time imaging SGE prototype system.

Specification	Proposed system
Dimensions / Weight	$108 \times 108 \times 60 \text{ mm}^3 / 0.7 \text{ kg}$
Maximum Gel Size	$100 \times 60 \text{ mm}^2$
Buffer Consumption	60 mL
LED Light	Blue (center wavelength: 465 nm $\pm$ 10 nm)
LED Configuration	Array of 18 high-power LEDs
Viewing Surface Dimensions	$100 \times 100 \text{ mm}^2$
Amber Filter	$100 \times 100 \text{ mm}^2 / \text{Center wavelength: } 520 \text{ nm}$
Image Resolution	3024 $\times$ 4032 (12 MP), 8-bit
Input Voltage	DC 24 V
Adjustable Output Voltage	DC 24–140 V with 1 V increments
Maximum Output Power	90 W

voltage of 140 V (electric field strength: 17.5 V/cm). **Fig. 4** illustrates the temporal evolution of the temperature distribution inside the SGE tank.

In the FEM simulations (**Fig. 4A**), temperature increased gradually over time, with the upper region showing the highest thermal accumulation. The upper temperature increased from 41.1 °C to 43.8 °C, while the central lower region (gel placement area) showed a gradual increase from 34.1 °C to 37.9 °C. This spatial gradient highlights the effective heat dissipation in the lower region, facilitated by the quartz glass plate, and the localized heat retention in the upper region due to the low thermal conductivity of the UV-curable resin. Experimental measurements using an E6-xt infrared thermal imager (**Fig. 4B**) confirmed these trends. The upper region reached 43.8 °C, consistent with simulation predictions, while temperatures in the lower gel region ranged from 33.8 °C to 37.6 °C. Notably, the system maintained temperatures below 45 °C (upper region) and 40 °C (gel area) during 15 min of operation at 140 V, confirming robust passive thermal management. Minor deviations between simulated and measured values (< 1 °C) are likely due to unmodeled convective cooling or variations in material properties. Both simulation and experimental results showed consistent temperature patterns: elevated heat near the electrodes and controlled thermal profiles in the gel region. This stability, achieved through the quartz glass plate, validates the ability of our design to minimize heat accumulation in critical areas. The results demonstrate that our SGE tank effectively balances high electric field strength operation with thermal safety, enabling rapid nucleic acid separation without the risk of gel melting.

In addition, the robust passive temperature control of our SGE tank enables improved nucleic acid separation efficiency under high electric field strength. As shown in **Fig. 5**, at an operation voltage of 100 V, the optimized SGE prototype system achieved clear separation of heat shock protein genes (HSP70, 2000 bp, 10 ng/μL, 5 μL) in 12 min, whereas the traditional SGE system [40] required 30 minutes to achieve comparable resolution. This accelerated performance is due to the optimized tank design, including flat platinum-titanium alloy electrodes that ensure electric field uniformity while generating a significantly higher field strength (12.5 V/cm vs. 5.0 V/cm in traditional systems). The increased field strength directly reduces separation time by 60 % while maintaining resolution, demonstrating superior operating efficiency. These results conclusively validate the ability of our SGE tank to achieve rapid, high-resolution electrophoresis.

### 3.3. Irradiation and emission evenness

Based on the theoretical derivation in **Section 2.3**, we built an LED panel and performed irradiation experiments by varying the distance between the panel and the gel from 5 mm to 30 mm in 5 mm increments. We then recorded the pixel uniformity of the captured images to validate our calculations. The irradiation maps at different diffuser heights are shown in **Fig. 6**. As shown in **Fig. 7**, as  $z$  increases, the irradiation evenness improves, reaching a maximum of 82.29 % at  $z = 20$  mm, after which it begins to decrease. This trend closely matches the theoretical predictions, confirming both the soundness and practical applicability of our design.

To further evaluate irradiation evenness, we used the fabricated LED array ( $100 \times 60 \text{ mm}^2$ ) to image a 1 % gel ( $60 \times 60 \text{ mm}^2$ ) without any samples. This setting provides full coverage while mitigating edge effects. Under uniform irradiation, the background signal of the gel should also be uniform. As shown in **Fig. 8A**, the imaging area was divided into 169 ( $13 \times 13$ ) subregions, and their grayscale values (mean = 28, std = 0.38) yielded a relative standard deviation (RSD) of 1.38 % ( $n = 169$ ), confirming irradiation evenness. Next, a DNA marker containing six dsDNA fragments (100, 200, 500, 750, 1000, 2000 bp) was loaded onto 12 lanes of the same gel and electrophoresed for 15 min (**Fig. 8B**). The locations of the DNA bands were uniformly distributed in the imaging area, and therefore we calculated the RSDs ( $n = 12$ ) of the gray values of

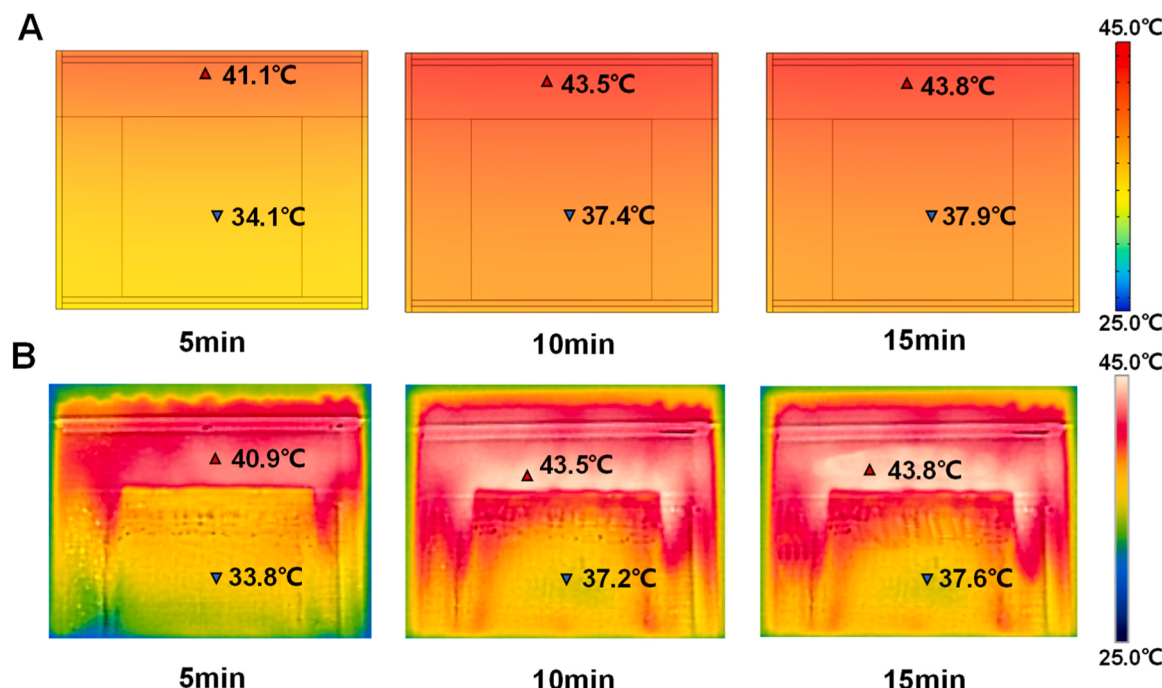


**Fig. 4.** Temporal variation of the temperature distribution in the SGE tank under a maximum voltage of 140 V (corresponding to an electric field strength of 17.5 V/cm). (A) The results of the FEM simulations. (B) Practical measured temperature maps obtained using an E6-xt infrared thermal imager.

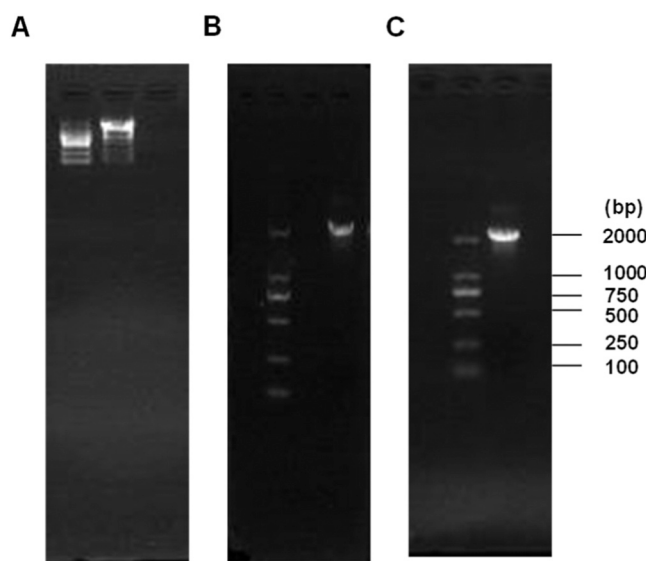


**Fig. 5.** Screening of heat shock protein genes (HSP70) in kelp using the same operation voltage setting of 100 V, traditional SGE system for 12 min @ 5.0 V/cm (A), 30 minutes @ 5.0 V/cm (B), and using our SGE tank for 12 min @ 12.5 V/cm(C).

these bands to evaluate the emission evenness (Fig. 8B and Table S4). The DNA bands were uniformly distributed, and their grayscale values had RSDs ( $n = 12$ ) ranging from 4.96 % to 8.89 %, indicating acceptable emission evenness (Table S4).

#### 3.4. Online DNA detection and quantification

After validating the optical performance of our real-time imaging SGE system, we performed electrophoresis using a DNA marker containing fragments of 100, 250, 500, 750, 1000, and 2000 bp. All fragments were at a concentration of 10 ng/ $\mu$ L, except the 750 bp fragment,

which was at 15 ng/ $\mu$ L. A 5  $\mu$ L DNA marker was loaded onto a 1 % agarose gel, and electrophoresis was conducted at 100 V for 15 min. Images were captured every 3 min with an exposure time of 0.6 s [31]. As shown in Fig. 9, we successfully tracked DNA migration in real time to identify the optimal electrophoresis endpoint. All six bands were clearly resolved at 12 min; however, by 15 min, band dispersion reduced the 2000 bp signal (red box), indicating that the run should ideally be stopped at 12 min.

Next, we conducted DNA quantification using a series of 5  $\mu$ L DNA marker solutions (0.03–50.00 ng/ $\mu$ L, CEBP fragment of 1200 bp) loaded onto a 1 % agarose gel. To minimize photobleaching and preserve sensitivity, endpoint detection was performed at 12 min, a time point previously verified to avoid band diffusion (Fig. 9). After electrophoresis, grayscale analysis of the gel images (Figures S2 – S3) provided intensity data for DNA concentrations ranging from 0.08 to 50.00 ng/ $\mu$ L.

A strong linear correlation was observed between fluorescence intensity and DNA concentration in the range of 0.08–10.00 ng/ $\mu$ L. Using the least squares method and Eq. (11), we modeled the relationship as:  $y = 52.06 + 16.19c$ , with an  $R^2$  value of 0.998 and a root mean square error (RMSE) of 2.258, indicating excellent linearity (Fig. 10). Based on the linear calibration curve and the standard deviation of blank measurements ( $s = 0.38$ , from Fig. 8), and using a sensitivity ( $b$ ) of 16.19 and a confidence factor ( $k$ ) of 3 in Eq. (10), the system achieved a LOD of 0.07 ng/ $\mu$ L. Repeatability was confirmed by calculating the relative standard deviation (RSD) across multiple runs, with all values below 1.30 % (Table S5). These results demonstrate the potential of our real-time imaging SGE system for rapid DNA separation and accurate quantitative analysis.

#### 3.5. Rice receptor protein kinase genes detection using the phone integrated system

To simplify user interaction, we developed a smartphone application called “iSGE,” available as both a cross-platform WeChat mini-program and an Android app. The app connects to the system via Bluetooth and provides an intuitive interface for setting parameters such as voltage and

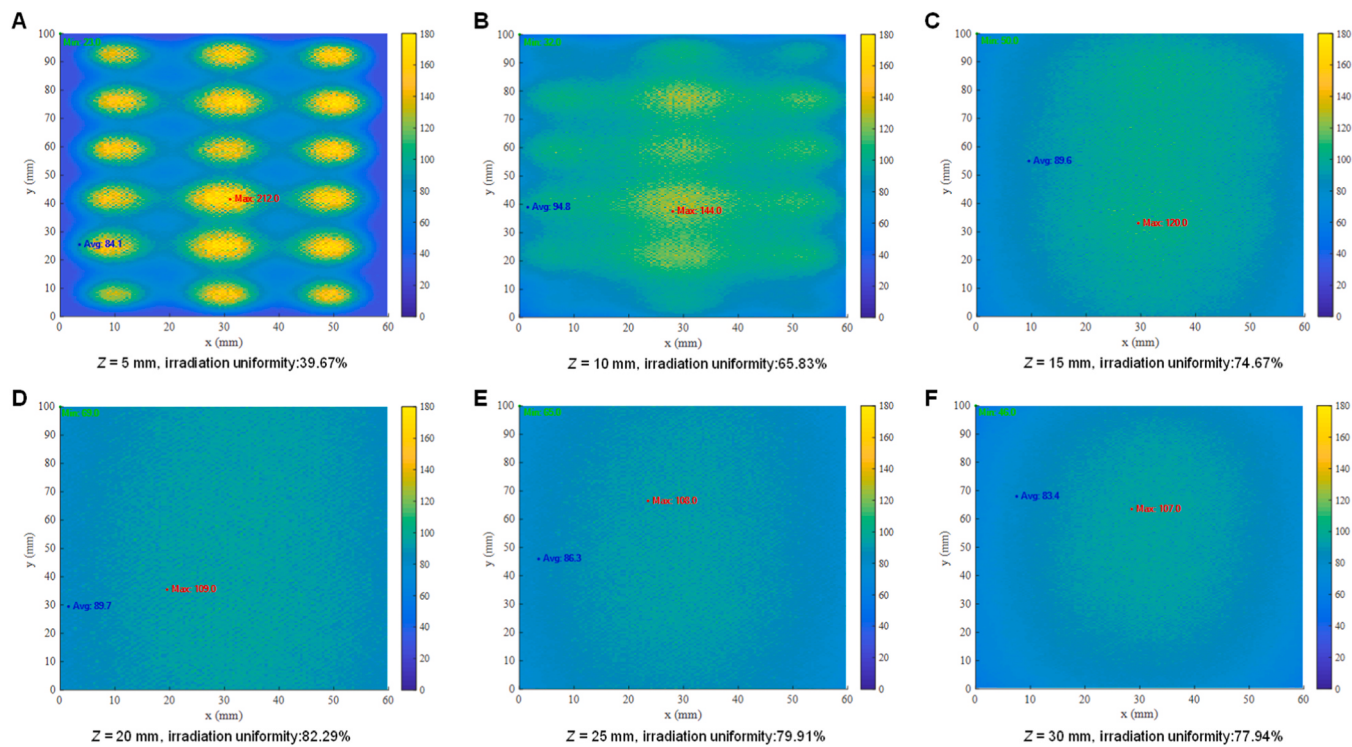


**Fig. 6.** The irradiation measurement results of the diffuser at different height  $z$ . (A)  $z = 5$  mm; (B)  $z = 10$  mm; (C)  $z = 15$  mm; (D)  $z = 20$  mm; (E)  $z = 25$  mm; (F)  $z = 30$  mm.

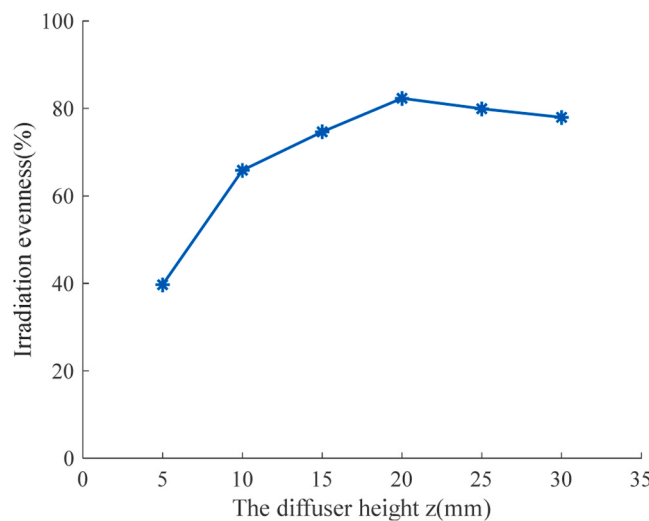


**Fig. 7.** Relationship between the irradiation evenness and the diffuser height ( $z$ ).

runtime, while also supporting real-time imaging and video recording. The source code for the app is provided in the [supplementary materials](#).

To assess its utility in molecular biology research, we used the system to detect rice receptor protein kinase genes (CERK1 and CEBiP), which form receptor complexes that activate downstream immune signaling pathways [41]. Identifying and characterizing these genes is critical for developing disease-resistant rice varieties through genetic engineering or selective breeding. As shown in Fig. 11, users connect to the BT04-E module in the Bluetooth interface (Fig. 11A) before setting the time and voltage in the electrophoresis operation interface (Fig. 11B). Pressing Start electrophoresis activates the run (Fig. 11C), and real-time imaging can be accessed by selecting Electrophoresis imaging (Fig. 11D). A

supplementary demonstration video is included in the attachment files to showcase the performance of the prototype system. The results confirm the effectiveness of our system in screening CERK1 and CEBiP within 12 min at 100 V, highlighting its potential to facilitate and accelerate molecular biology research.

#### 4. Discussion

In this work, we have addressed several critical challenges associated with portable real-time imaging SGE systems, including insufficient irradiation evenness, excessive Joule heating at high electric field strength, and inefficient post-processing requirements. Our proposed system overcomes these issues through an integrated design featuring a custom SGE tank optimized for efficient passive heat dissipation at high electric field strength, uniform large-area LED irradiation, and simplified real-time fluorescence imaging. This approach delivers rapid separations, improved sensitivity, and substantial cost savings, bridging theoretical innovation and practical engineering to realize a portable and user-friendly real-time imaging SGE solution.

Irradiation evenness is critical to ensure repeatability, sensitivity, and accuracy of DNA detection in online imaging gel electrophoresis [31]. Insufficient irradiation evenness can lead to local variations in fluorescence signals, introducing quantitative errors and compromising the reliability of experimental results [29]. Our system achieves highly uniform irradiation through an optimized LED panel design and precise optical alignment. Both the simulation and experimental data show that the RSD of the background signal intensity remains exceptionally low (1.38 % in the  $13 \times 13$  subregions) (Fig. 8A), confirming excellent irradiation evenness across the imaging area. Importantly, when we assessed signal consistency using a six-band DNA marker loaded across 12 lanes, the RSD values of band intensity ranged from 4.96 % to 8.89 % (Fig. 8B and Table S4), highlighting consistent emission evenness. This evenness is particularly advantageous for the detection of low concentration samples [31], as it minimizes local intensity variations that could otherwise affect the LOD. The integration of a smartphone-based

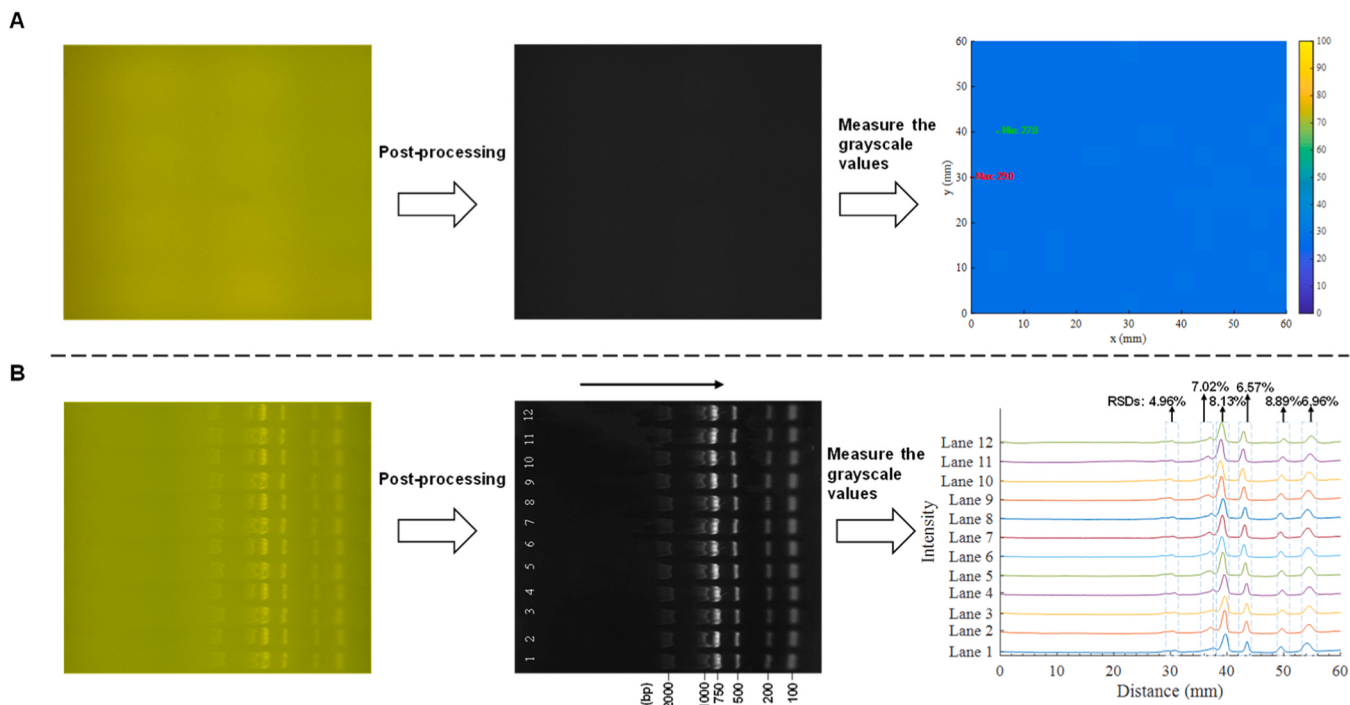


**Fig. 8.** Evaluation of irradiation and emission evenness. (A) Grayscale of the background signal of the irradiation of the gel without sample loading. The imaging area was  $60 \times 60 \text{ mm}^2$ , which was divided into  $13 \times 13$  subregions. The scale bar indicates the gray level of the background signal from 0 to 100. The mean gray value of the blank measurements is 28, with a standard deviation of 0.38. (B) Gel image of 12 parallel samples of  $5 \mu\text{L}$  DNA marker (100, 200, 500, 750, 1000, and 2000 bp). The black arrow indicates the direction of electrophoretic migration. The right side is the chromatogram after gel image conversion. Each group of peaks in the dashed box represents one of the 100, 200, 500, 750, 1000, and 2000 bp DNA. The RSDs ( $n = 12$ ) were calculated based on the peak areas of 12 peaks in the box.

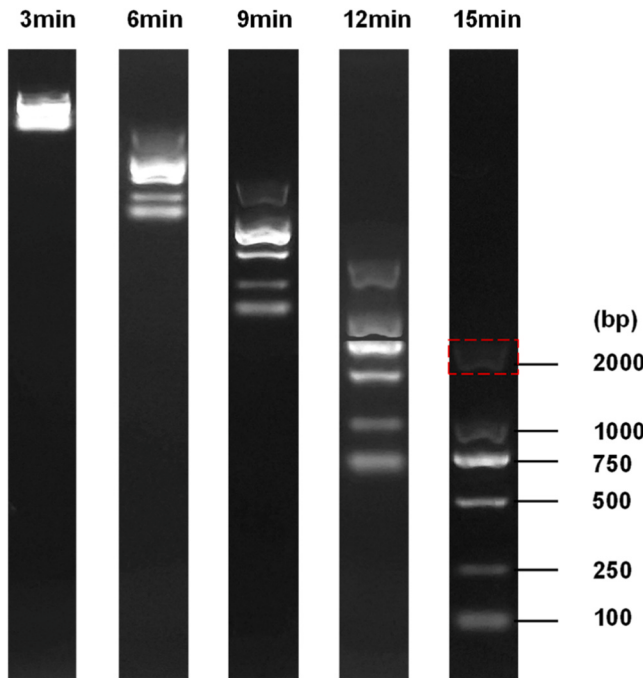


**Fig. 9.** Real-time monitoring of the 15-minute separation process of the DNA marker. The red box highlights the low sensitivity of the detection of 2000 bp DNA due to band diffusion during electrophoresis.

imaging system further enhances usability. The built-in CMOS sensor of the iPhone 13 Pro, combined with a 520 nm bandpass filter, provides high-resolution, real-time imaging with minimal post-processing. This approach eliminates the need for complex optical alignments or external

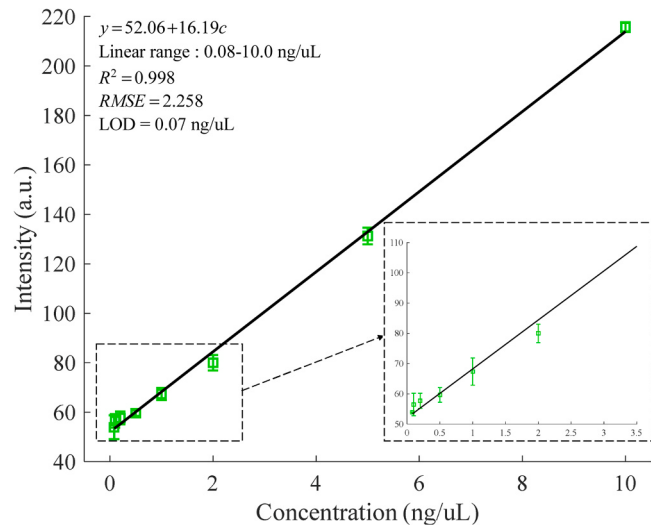


**Fig. 10.** Quantitative DNA concentration analysis using our portable real-time imaging SGE system. The linear relationship was established based on the concentration (0.08 ng/uL - 10.00 ng/uL) of CEBiP and the fluorescence band intensity. Error bars indicate the standard deviations of triplicate tests.

imaging devices, making the system more accessible and user-friendly.

Another advancement is the robust thermal management strategy. Effective heat dissipation is essential to maintain gel integrity and separation efficiency, especially at high electric field strength. By embedding a quartz glass plate and flat platinum-titanium alloy electrodes in the tank, we achieve efficient passive heat dissipation, enabling stable operation at electric field strength as high as  $17.5 \text{ V/cm}$  without risking gel melting. FEM simulations and experimental measurements confirmed that the system maintains temperatures below  $45^\circ\text{C}$  in the

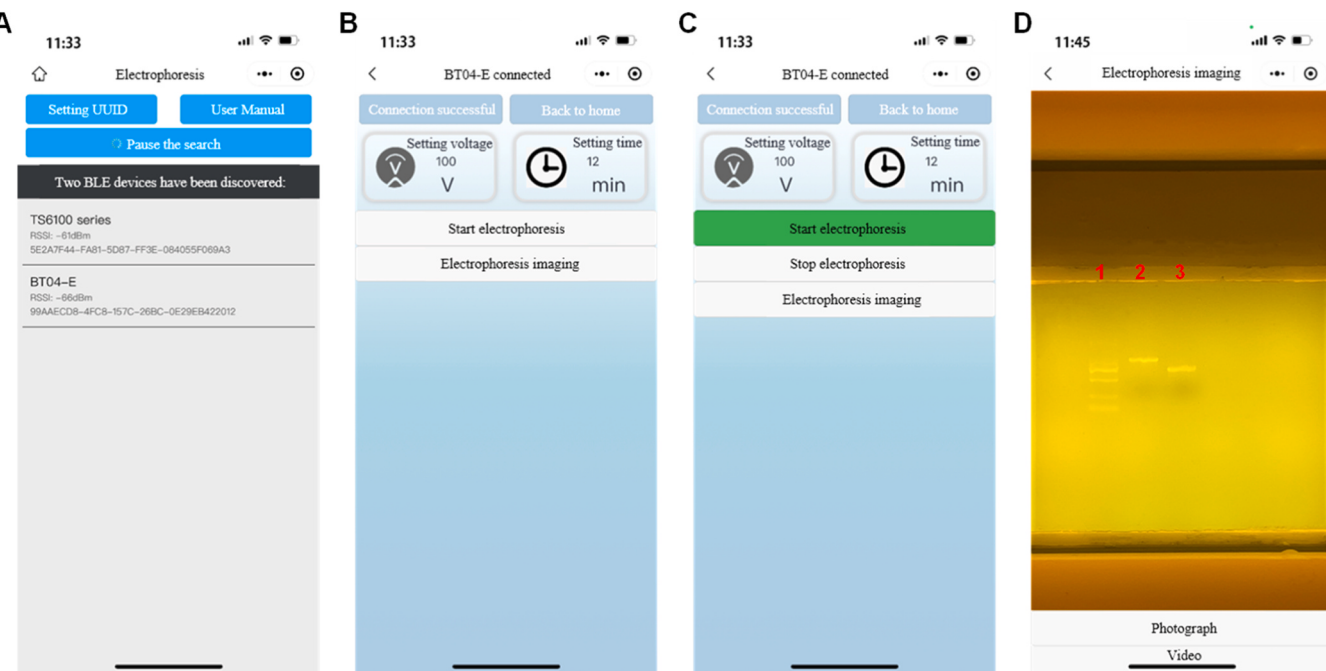


**Fig. 11.** A real-time monitoring demo of our portable imaging SGE system. (A) Bluetooth connection setting, (B) electrophoresis operation setting, (C) electrophoresis processing control, and (D) real-time electrophoresis imaging, the columns “1–3” are DNA markers, CERK1, and CEBiP respectively.

upper region and 40 °C in the gel region during operation (Fig. 4). This robust thermal management enables accelerated nucleic acid separation through the use of high electronic field strength, which reduces the runtime for the resolution of heat shock protein genes (HSP70) from 30 min in traditional SGE system to as little as 12 min (Fig. 5). Such accelerated separation not only increases throughput but also addresses the needs of POCT and other rapid diagnostic scenarios [42].

The real-time imaging capability of our system enables dynamic monitoring of DNA separation, allowing users to identify the optimal endpoint for electrophoresis. As shown in Fig. 9, the system successfully tracked the migration of a DNA ladder (100–2000 bp) in real-time, with all bands clearly resolved within 12 min. This feature not only improves efficiency but also minimizes band diffusion, which can affect detection sensitivity with longer runtimes. In terms of analytical performance, our system demonstrates reliable DNA quantification over a wide dynamic range (0.08–10.00 ng/μL) with an LOD of 0.07 ng/μL (Fig. 10). The high coefficient of determination ( $R^2 = 0.998$ ) and low root mean square error (RMSE = 2.258) confirm the accuracy of our method. However, fluorescence signal saturation was observed at concentrations above 10.00 ng/μL, suggesting the need for sample loading adjustments for high concentration applications [30]. These features, coupled with the ability to run up to 12 samples per batch, significantly increase both sensitivity and throughput compared to traditional instruments. In addition to performance improvements, integration with the “iSGE” app

provides an intuitive user interface to control key parameters such as voltage and runtime, and facilitates real-time imaging and video recording (Fig. 11). This capability eliminates traditional post-electrophoresis steps, such as gel staining and separate visualization, significantly streamlining the analytical workflow. Furthermore, the compact and cost-effective design of our system (10.8 × 10.8 × 6.0 cm<sup>3</sup>, 0.7 kg, approximately \$65 cost) offers a practical solution for resource-limited institutions.

As summarized in Table 3, our proposed SGE system offers comparable performance or partially superior performance to previously reported platforms, such as the intrinsic fluorescence imaging (IFI)-based gel electrophoresis chip (GEC) system [30], the polyacrylamide gel electrophoresis (PAGE) IFI platform [29], and the online polyacrylamide gel electrophoresis (OPAGE) platform [31], in terms of runtime, sensitivity, imaging area, and affordability. Notably, our system reduces electrophoresis runtime by approximately 60 % compared to traditional SGE system, shortening a typical 30-minute experiment to just 12 min at the same voltage (100 V). Moreover, its large imaging area (100 × 60 mm<sup>2</sup>) and smartphone-based detection capabilities offer advantages over systems with limited imaging zones or complex optical setups. Stable electrophoretic separations under reduced buffer volumes (16 times lower than traditional SGE systems) and relatively high electric field strength (12.5 V/cm) are achieved through several optimized design features. These include platinum-titanium planar electrodes

**Table 3**

Comparison of our SGE system, IFI-GEC system, PAGE-IFI platform, OPAGE platform, and traditional SGE system.

Metric	Our SGE system	IFI GEC system [30]	PAGE IFI platform [29]	OPAGE platform [31]	Traditional SGE system [40]
Runtime of GE [min]	12	10	45	45	30
Dynamic ranges [ng/μL]	0.08–10.00	20.00–2000.00	30.00–10000.00	0.10–12.50	-
LOD [ng/μL]	0.07	10.00	20.00	0.08	-
Length of channel/lane [mm]	60	20	70	60	60
Online dynamic imaging (ODI)	yes	yes	yes	yes	no
Gel consumption [mL]	25.0	0.24	-	-	25.0
Buffer consumption [mL]	60	10	-	-	~ 1000
Size [cm <sup>3</sup> ]	10.8 × 10.8 × 6.0	15.0 × 15.0 × 38.0	14.0 × 12.0 × 10.0	-	30.0 × 17.0 × 8.0
Price [\$]	~ \$65.00*	-	-	-	≥ \$1500.00

\* Price does not include the smartphone

( $100 \times 20 \times 1 \text{ mm}^3$ ) producing a uniform electric field across an 80 mm gap, quartz glass plates ( $60 \times 100 \times 1 \text{ mm}^3$ ) embedded in the gel tank for efficient Joule heat dissipation, and a carefully introduced 20 mm gap between the negative electrode and the edge of the quartz plate to minimize interference from hydrogen bubbles generated during high-voltage electrolysis. The system achieves a LOD of 0.07 ng/ $\mu\text{L}$ , enabled by uniform LED irradiation, the high optical clarity of the quartz glass, and a large imaging area captured via smartphone. Experimental results and supplementary videos confirm the effectiveness of these design strategies, demonstrating stable and reliable separation performance.

Compared to advanced capillary electrophoresis (CE) and capillary gel electrophoresis (CGE) technologies, which offer automated operation, rapid separation, high sensitivity, and reduced reagent usage but typically require expensive, technically demanding equipment and high-voltage (kV-range) power supplies [43–45], our proposed SGE system remains significantly more affordable ( $\sim \$65$ ), simpler, and easier to operate. The demonstrated benefits, including reduced buffer consumption, rapid analysis, and real-time smartphone-based monitoring, make our system particularly suitable for widespread adoption. Furthermore, its open source design ensures reproducibility and accessibility, providing a valuable reference for researchers in resource-limited environments and those developing portable, low-cost, miniaturized molecular detection technologies.

Despite its many advantages, the current system has several limitations. First, it lacks integrated real-time data analysis software, requiring users to rely on external tools such as Image J for quantitative analysis. Second, the post-electrophoresis cleaning process remains manual, which could be automated in future iterations to further enhance usability. Finally, integration of the system with sample preparation technologies, such as PCR or isothermal amplification [46,47], could expand its applicability in clinical diagnostics and field research.

## 5. Conclusions

In this work, we have developed a portable real-time imaging SGE system that addresses several challenges in POCT nucleic acid analysis. By integrating a custom SGE tank with effective passive heat dissipation, a flat panel LED array for uniform large area irradiation, and a smartphone-based camera for real-time image acquisition, the system achieves rapid separation and highly sensitive fluorescence detection in a highly compact design.

Compared to traditional SGE systems, our prototype significantly reduces typical runtime (from 30 min to as little as 12 min) while maintaining excellent band resolution. System components, including platinum-titanium alloy electrodes and an embedded quartz glass plate, provide uniform electric fields and robust heat dissipation, allowing operation at high electric field strength without the risk of gel melting. Additionally, the custom LED panel and 520 nm filter provide uniform fluorescence excitation across a  $60 \times 60 \text{ mm}^2$  gel, minimizing artifacts and improving detection reliability. The integrated smartphone interface provides an easy-to-use workflow: researchers can control voltage, runtime, and imaging parameters via the smartphone app while observing the electrophoresis progress in real-time. The ability to dynamically track fluorescent band migration eliminates post-processing steps, reducing overall experimental time and simplifying nucleic acid analysis workflows. Evaluation with DNA marker samples and receptor protein kinase genes in rice demonstrated that the system provides robust quantitative accuracy (LOD of 0.07 ng/ $\mu\text{L}$ ). These features, combined with its compact size ( $108 \times 108 \times 60 \text{ mm}^3$ ), light weight (0.7 kg), and low cost ( $\sim \$65$ ), make it particularly suitable for on-site testing and resource-limited settings.

Overall, this portable real-time imaging SGE system provides an integrated, efficient, and cost-effective solution to the challenges of POCT genetic analysis. Future work will focus on automating data analysis, integrating additional sample preparation steps, and further extending

the capabilities of the system to meet broader testing needs. The design principles outlined here can serve as a valuable reference framework for the development of similar portable detection platforms.

## CRediT authorship contribution statement

**Fan Min:** Writing – review & editing, Writing – original draft, Validation, Methodology. **Li Jianxing:** Visualization, Software, Data curation. **Wang Wu:** Writing – review & editing, Methodology, Conceptualization. **Luo Kan:** Writing – review & editing, Writing – original draft, Supervision, Project administration, Methodology, Conceptualization. **Chen Yu:** Writing – original draft, Software, Methodology, Data curation, Conceptualization.

## Declaration of Competing Interest

The authors declare that they have no known competing financial interests or personal relationships that could have appeared to influence the work reported in this paper.

## Acknowledgements

This research was supported by Grant 2024-G-014 from the Fuzhou Science and Technology Bureau, China, Grant 2023C007 from the Ningde Science and Technology Bureau, China, and Grant 61601124 from the NSFC, China.

## Appendix A. Supporting information

Supplementary data associated with this article can be found in the online version at doi:[10.1016/j.snb.2025.137905](https://doi.org/10.1016/j.snb.2025.137905).

## Data availability

Data will be made available on request.

## References

- [1] N.C. Stellwagen, Electrophoresis of DNA in agarose gels, polyacrylamide gels and in free solution, *Electrophoresis* 30 (S1) (2009) S188–S195.
- [2] Y. Zhang, Y. Wang, B. Zhang, P. Li, Y. Zhao, Methods and biomarkers for early detection, prediction, and diagnosis of colorectal cancer, *Biomed. Pharmacother.* 163 (2023) 114786.
- [3] K.A.B. Benites, W.A. García-Quispes, RFLP-inator: interactive web platform for *in silico* simulation and complementary tools of the PCR-RFLP technique, *IEEE/ACM Trans. Comput. Biol. Bioinf.* 21 (6) (2024) 2510–2517.
- [4] H.M. Rehman, N. Yousaf, S.M. Hina, T. Nadeem, M.A. Ansari, A. Chaudry, I. Kafait, S. Khalid, A.R. Alanzi, H. Bashir, Design and computational analysis of a novel Azurin-BR2 chimeric protein against breast cancer, *Toxicol. Res.* 13 (6) (2024) tfae179.
- [5] H. Shuaib, Z. Saleem, M. Alshahran, M. Suliman, U. Hani, T. Nadeem, S. Tahir, M. Akram, O. Samreen, H. Bashir, Development and bioactivity assessment of a recombinant pseudomonas aeruginosa Azurin-BR2 Peptide fusion protein: a novel approach to cancer immunotherapy, *J. Biol. Regul. Homeost. Agents* 38 (2024) 5573–5581.
- [6] H. Nölvak, M. Truu, J. Truu, Evaluation of quantitative real-time PCR workflow modifications on 16S rRNA and tetA gene quantification in environmental samples, *Sci. Total Environ.* 426 (2012) 351–358.
- [7] D.-D. Zuo, H.-T. Sun, L. Yang, M.-L. Zheng, J. Zhang, D.-L. Guo, Hydrogen peroxide priming triggers splicing memory in grape berries, *Plant Mol. Biol.* 114 (6) (2024) 129.
- [8] R. Kalendar, K. Ivanov, O. Samuilova, U. Kairov, A. Zamyatnin, Isolation of high-molecular-weight DNA for long-read sequencing using a high-salt gel electroelution trap, *Anal. Chem.* 95 (2023) 17818–17825.
- [9] K. Motohashi, Development of highly sensitive and low-cost DNA agarose gel electrophoresis detection systems, and evaluation of non-mutagenic and loading dye-type DNA-staining reagents, *PLOS ONE* 14 (9) (2019) e0222209.
- [10] J. B.M., V. N.A., G. Hua, P. N.G., T. W.A., 3D printed microfluidic devices for microchip electrophoresis of preterm birth biomarkers, *Anal. Chem.* 91 (11) (2019) 7418–7425.
- [11] A. S.M., D. C.A., M.R. Scott, PolyJet-based 3D printing against micromolds to produce channel structures for microchip electrophoresis, *ACS Omega* 7 (15) (2022) 13362–13370.

- [12] Z. Li, J. Huang, B. Yang, Q. You, S. Sekine, D. Zhang, Y. Yamaguchi, Miniaturized gel electrophoresis system for fast separation of nucleic acids, *Sens. Actuators B Chem.* 254 (2018) 153–158.
- [13] Y.K. Jung, J. Kim, R.A. Mathies, Microfluidic hydrogel arrays for direct genotyping of clinical samples, *Biosens. Bioelectron.* 79 (2016) 371–378.
- [14] V.D. Nguyen, H.V. Nguyen, K.H. Bui, T.S. Seo, Smart phone-powered capillary electrophoresis on a chip for foodborne bacteria detection, *Sens. Actuators. B Chem.* 301 (C) (2019) 127108.
- [15] S. Z.D., R. Binayak, T. M.M., G. K.W., A. B.S., Rapid fabrication of a poly (dimethylsiloxane) microfluidic capillary gel electrophoresis system utilizing high precision machining, *Lab a chip* 3 (2) (2003) 93–99.
- [16] L. Ralph, K. A.L., H. Ari, M. Minna, A. Anne, P. Mikko, R. S.J., A. M.R., K. Marika, U. Sanna, H. Leena, K. N.T., S. Harri, S. Hans, Disposable roll-to-roll hot embossed electrophoresis chip for detection of antibiotic resistance gene *mecA* in bacteria, *Lab a chip* 12 (2) (2012) 333–339.
- [17] R.S. Rush, A.S. Cohen, B.L. Karger, Influence of column temperature on the electrophoretic behavior of myoglobin and alpha-lactalbumin in high-performance capillary electrophoresis, *Anal. Chem.* 63 (14) (1991) 1346–1350.
- [18] A. Cifuentes, X. Xu, W.T. Kok, H. Poppe, Optimum conditions for preparative operation of capillary zone electrophoresis, *J. Chromatogr. A* 716 (1) (1995) 141–156.
- [19] J.A. Luckey, L.M. Smith, Optimization of electric field strength for DNA sequencing in capillary gel electrophoresis, *Anal. Chem.* 65 (20) (2002) 2841–2850.
- [20] E. David, S. David, L. Dongqing, Joule heating and heat transfer in poly (dimethylsiloxane) microfluidic systems, *Lab a Chip* 3 (3) (2003) 141–149.
- [21] S.H. Sajjadi, E.K. Goharshadi, H. Ahmadzadeh, Heat dissipation in slab gel electrophoresis: The effect of embedded TiO<sub>2</sub> nanoparticles on the thermal profiles, *J. Chromatogr. B* 1118–1119 (2019) 63–69.
- [22] B.O. Eriksson, I.L. Skuland, N.D. Marlin, M.B.O. Andersson, L.G. Blomberg, In-line application of electric field in capillary separation systems: Joule heating, pH and conductivity, *Talanta* 75 (1) (2008) 83–90.
- [23] J. Yan, C.-G. Guo, X.-P. Liu, F.-Z. Kong, Q.-Y. Shen, C.-Z. Yang, J. Li, C.-X. Cao, X.-Q. Jin, A simple and highly stable free-flow electrophoresis device with thermoelectric cooling system, *J. Chromatogr. A* 1321 (2013) 119–126.
- [24] N. Mukhitov, L. Yi, A.M. Schrell, M.G. Roper, Optimization of a microfluidic electrophoretic immunoassay using a Peltier cooler, *J. Chromatogr. A* 1367 (2014) 154–160.
- [25] Q. Pan, K.A. Yamauchi, A.E. Herr, Controlling dispersion during single-cell polyacrylamide-gel electrophoresis in open microfluidic devices, *Anal. Chem.* 90 (22) (2018) 13419–13426.
- [26] M. Bercovici, G.V. Kaigala, C.J. Backhouse, J.G. Santiago, Fluorescent carrier ampholytes assay for portable, label-free detection of chemical toxins in tap water, *Anal. Chem.* 82 (5) (2010) 1858–1866.
- [27] J.Z. Pan, P. Fang, X.-X. Fang, T.-T. Hu, J. Fang, Q. Fang, A low-cost palmtop high-speed capillary electrophoresis bioanalyzer with laser induced fluorescence detection, *Sci. Rep.* 8 (1) (2018) 1791.
- [28] J. Roegener, P. Lutter, R. Reinhardt, M. Blüggel, H.E. Meyer, D. Anselmetti, Ultrasensitive detection of unstained proteins in acrylamide gels by native UV Fluorescence, *Anal. Chem.* 75 (1) (2003) 157–159.
- [29] Z. Yu, Y. Cao, Y. Tian, W. Ji, K.-E. Chen, Z. Wang, J. Ren, H. Xiao, L. Zhang, W. Liu, L. Fan, Q. Zhang, C. Cao, Real-time and quantitative protein detection via polyacrylamide gel electrophoresis and online intrinsic fluorescence imaging, *Anal. Chim. Acta* (2024) 342219.
- [30] J. Xue, Y. Cao, G. Zha, Z. Yu, Y. Wang, W. Liu, J. Ren, H. Xiao, Q. Zhang, L. Wei, C. Cao, Quadruple UV LED array for facile, portable, and online intrinsic fluorescent imaging of protein in a whole gel electrophoresis chip, *Anal. Chem.* 95 (15) (2023) 6193–6197.
- [31] Z. Wang, Y. Cao, Z. Yu, Y. Tian, J. Ren, W. Liu, L. Fan, Q. Zhang, C. Cao, High-resolution nucleic acid detection using online polyacrylamide gel electrophoresis platform, *J. Chromatogr. A* 1713 (2024) 464571.
- [32] C. Tao, B. Yang, Z. Li, D. Zhang, Y. Yamaguchi, Real-time tracking of DNA fragment separation by smartphone, *JoVE* (124) (2017) e55926.
- [33] E.N. Cunha, M.F.B. de Souza, D.C.F. Lanza, J.P.M.S. Lima, A low-cost smart system for electrophoresis-based nucleic acids detection at the visible spectrum, *PLoS ONE* 15 (10) (2020) e0240536.
- [34] M. Salem, O. Aldabbagh, Numerical Solution to Poisson's equation for estimating electrostatic properties resulting from an axially symmetric Gaussian charge density distribution: charge in free space, *Mathematics* 12 (13) (2024).
- [35] X. Jingjing, Z. Qiang, C. Jun, T. Youli, Z. Genhan, L. Xiaoping, L. Weiwen, W. Yuxing, G. Dingkun, C. Chengxi, Gel electrophoresis chip using joule heat self-dissipation, short run time, and online dynamic imaging, *Anal. Chem.* 94 (4) (2021).
- [36] I. Moreno, M. Avendaño-Alejo, R.I. Tzonchev, Designing light-emitting diode arrays for uniform near-field irradiance, *Appl. Opt.* 45 (10) (2006) 2265–2272.
- [37] Y. Huang, J. Ma, Laser and LED HYbrid Plant Lighting System Design Based on the Particle Swarm Algorithm, *Appl. Sci.* 10 (21) (2020).
- [38] F. Wu, S. Li, X. Zhang, W. Ye, A design method for LEDs arrays structure illumination, *J. Disp. Technol.* 12 (2016), 1–1.
- [39] J. Krupčík, P. Májek, R. Gorovenko, J. Blaško, R. Kubinec, P. Sandra, Considerations on the determination of the limit of detection and the limit of quantification in one-dimensional and comprehensive two-dimensional gas chromatography, *J. Chromatogr. A* 1396 (2015) 117–130.
- [40] WIX-midiDNA Multipurpose Horizontal Electrophoresis Cell. (<http://www.wixscientific.com/plus/view.php?aid=46>).
- [41] T. Shinya, N. Motoyama, A. Ikeda, M. Wada, K. Kamiya, M. Hayafune, H. Kaku, N. Shibuya, Functional characterization of CEBP and CERK1 homologs in arabidopsis and rice reveals the presence of different chitin receptor systems in plants, *Plant Cell Physiol.* 53 (10) (2012) 1696–1706.
- [42] X. Meng, X. Pang, J. Yang, X. Zhang, H. Dong, Recent advances in electrochemiluminescence biosensors for MicroRNA detection, *Small* 20 (13) (2023) 6.
- [43] M.S. Ferreira Santos, E. Kurfman, K. Zamuruyev, A.C. Noell, M.F. Mora, P.A. Willis, A voltage trade study for the design of capillary electrophoresis instruments for spaceflight, *Electrophoresis* 44 (1–2) (2023) 10–14.
- [44] J.P. Tran, J. Gao, C. Lansdell, B. Lorbettskie, M.J.W. Johnston, L. Wang, X. Li, H. Lu, A Comprehensive evaluation of analytical method parameters critical to the reliable assessment of therapeutic mRNA integrity by capillary gel electrophoresis, *Electrophoresis* (2025).
- [45] R.K. Harstad, M.T. Bowser, High-speed microdialysis-capillary electrophoresis assays for measuring branched chain amino acid uptake in 3T3-L1 cells, *Anal. Chem.* 88 (16) (2016) 8115–8122.
- [46] S.K. Jha, R. Chand, D. Han, Y.-C. Jang, G.-S. Ra, J.S. Kim, B.-H. Nahm, Y.-S. Kim, An integrated PCR microfluidic chip incorporating aseptic electrochemical cell lysis and capillary electrophoresis amperometric DNA detection for rapid and quantitative genetic analysis, *Lab a Chip* 12 (21) (2012) 4455–4464.
- [47] J. Wang, H. Jiang, L. Pan, X. Gu, C. Xiao, P. Liu, Y. Tang, J. Fang, X. Li, C. Lu, Rapid on-site nucleic acid testing: on-chip sample preparation, amplification, and detection, and their integration into all-in-one systems, *Front. Bioeng. Biotechnol.* 11 (2023).

**Kan Luo** received the B.S. degree from Shandong University in 2005 and the Ph.D. degree in instrument science and engineering from Southeast University, China, in 2015. He is currently an associate professor with the School of Electronic, Electrical Engineering and Physics, Fujian University of Technology. His main research interests include biomedical device, biosignal processing, body sensor networks and machine learning.

**Yu Chen** received the B.S. degree from the Fujian University of Technology, Fujian, China, in 2022. He is currently pursuing the M.S. degree with the School of Mechanical and Automotive Engineering, Fujian University of Technology, Fuzhou, China. His main research interests include biomedical device, imaging analysis, and biosensors.

**Min Fan** received the B.S. degree from Fujian Normal University in 2018 and the Ph.D. degree in optical engineering from Fujian Normal University, China, in 2024. She is currently an associate professor at Fujian Provincial Key Laboratory for Advanced Micro-nano Photonics Technology and Devices, Institute for Photonics Technology, Quanzhou Normal University, China. Her research interests focus on the development of spontaneous Raman spectroscopy and surface-enhanced Raman spectroscopy-based optical biosensor for biomedical applications.

**Jianxing Li** received the B.S. degree from Harbin Engineering University in 1990 and the M.Sc. degree in Control Theory and Control Engineering from Central South University, China, in 2008. He is currently a professor with the School of Electronic, Electrical Engineering and Physics, Fujian University of Technology. His main research interests include control and filtering of networked systems, modelling, optimization and control of electrical systems, application of artificial intelligence, and application of embedded systems.

**Wu Wang** received the B.S. degree from Fujian Agriculture and Forestry University in 1996 and the Ph.D. degree in Electrical Machines and Electrical Appliances from Fuzhou University, China, in 2004. He is currently a professor with the College of Electrical Engineering and Automation, Fuzhou University. His main research interests include networked system control and filtering of networked systems, modelling, optimization and control of electrical systems, application research of artificial intelligence, and embedded systems.